

The University of Akron

IdeaExchange@UAkron

Williams Honors College, Honors Research
Projects

The Dr. Gary B. and Pamela S. Williams Honors
College

Spring 2021

Wetting Transition on 3D-printed Featured Surface

Hannah Pineault
hjp15@zips.uakron.edu

Follow this and additional works at: https://ideaexchange.uakron.edu/honors_research_projects



Part of the [Membrane Science Commons](#), and the [Polymer Science Commons](#)

Please take a moment to share how this work helps you [through this survey](#). Your feedback will be important as we plan further development of our repository.

Recommended Citation

Pineault, Hannah, "Wetting Transition on 3D-printed Featured Surface" (2021). *Williams Honors College, Honors Research Projects*. 1274.

https://ideaexchange.uakron.edu/honors_research_projects/1274

This Dissertation/Thesis is brought to you for free and open access by The Dr. Gary B. and Pamela S. Williams Honors College at IdeaExchange@UAkron, the institutional repository of The University of Akron in Akron, Ohio, USA. It has been accepted for inclusion in Williams Honors College, Honors Research Projects by an authorized administrator of IdeaExchange@UAkron. For more information, please contact mjon@uakron.edu, uapress@uakron.edu.

Wetting Transition of 3D-printed Featured Surfaces

Hannah Pineault

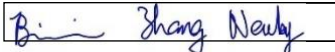
Department of Chemical, Biomolecular, and Corrosion
Engineering

Honors Research Project

Submitted to

*The Williams Honors College
The University of Akron*

Approved:

 Date: 4/19/2021

Honors Project Sponsor (signed)

Bi-min Zhang Newby

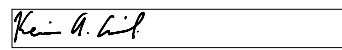
Honors Project Sponsor (printed)

R. Gitiafroz Date: 04/19/2021

Reader (signed)

Roya Gitiafroz

Reader (printed)

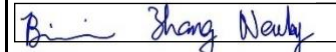
 Date: 4/19/2021

Reader (signed)

Kevin Cavicchi

Reader (printed)

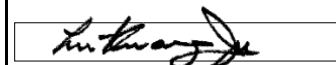
Accepted:

 Date: 4/19/2021

Honors Department Advisor (signed)

Bi-min Zhang Newby

Honors Department Advisor (printed)

 Date: 4/20/2021

Department Chair (signed)

Lu-Kwang Ju

Department Chair (printed)

Table of Contents

<i>Executive Summary</i>	3
<i>Introduction</i>	5
<i>Background</i>	6
<i>Experimental Methods</i>	8
<i>Data and Results</i>	9
<i>Discussion and Analysis</i>	12
<i>Literature Cited</i>	13
<i>Appendices</i>	15
Appendix A: Additional Figures/Tables	15
Appendix B: Statistical Analysis and Results	16

Executive Summary

The primary objective of this honors research project was to gain a better understanding of surface characteristics to produce a long-lasting superhydrophobic or superhydrophilic surface. In other words, when will a droplet of water remain on top of a featured surface and when does the transition occur to water filling the grooves of the surface? This research focused on how to best fabricate porous structures that would stay completely dry at all times by preventing the liquid from penetrating.

In particular, we followed the behaviors of water droplets placed on top of 3-D printed featured surfaces with various geometries and surface treatments. Cylindrical pillars in a hexagonal array were 3-D printed with varying pillar diameter (D) and height (H) as well as the spacing ratio (S/D). The as printed models, models oxidized using air plasma, and models treated with hydrophobic octadecyl trichlorosilane (OTS) were tested. Both the as printed and plasma treated models didn't retain water on top of the features due to their surfaces being hydrophilic, while the hydrophobic OTS treated models were able to prevent water droplets from penetrating down to the surface. The inversed features molded from the 3-D printed models using hydrophobic silicone elastomer also showed complete prevention of water drops from penetrating the features. Varying the geometry of the pillars had a significant effect in a majority of the cases across the various surface treatments on the transition. Meanwhile, the contact angle was affected by varying the pillar height but rarely by a change in diameter.

The 3D printer had size limitations, and to obtain the desired small features, the spacing was not varied and the height could only be varied slightly. In the future with a more capable 3D printer, it would be desirable to study surfaces with smaller pillar diameter, spacing, and varying heights, which would likely obtain more insightful results on the effects of features on liquid penetration. The 3D printer had additional printing limitations that resulted in the pillars having

rounded tops instead of the desired flat tops. That downward angle contributed to the droplet more easily wetting the surface. This is ideal for a hydrophilic surface, but a flat or concave top would create a more liquid repelling surface.

Insights gained from this project can potentially be applied to develop technology that can mitigate or even eliminate corrosion or can be used to trap water even in extreme conditions. Other useful applications would include self-cleaning surfaces, effective oil and water separation, water harvesting, anti-fogging and anti-fouling. Steps for further research would include investigating additional geometry dimensions and arrays, other liquids, and varying droplet volume. This research builds upon relevant studies and technical reports concerning droplet behavior and surface features.

Introduction

Hydrophobic and hydrophilic surfaces exist naturally, such as the water fern plant known as *Salvinia Molesta*, which repels water on its surface ^[1]. The super hydrophobicity of *Salvinia Molesta* is accomplished by having an egg-beater like shape top (Figure 1a-b) that consists of hydrophilic hair tips and a sophisticated hierarchical structure, trapping a layer of air in it, creating a buoyancy effect. Another example of a natural super-hydrophobic surface is the lotus leaf (Figure 1c). The small protrusions known as papillae's (Figure 1d) are coated with water-repellant wax crystals ^[2]. When compared to plants with similar features, the lotus leaf has high density and small diameter papillae's which contribute to it superior hydrophobicity ^[2].

Plants and animals utilize their hydrophobic and hydrophilic surfaces to repel or harvest water for their survival. Desert beetles like the *Stenocara Gracilipes*, are known to survive in the dessert environment by collecting water from fog using its unique back structure. Its back contains an array of hydrophilic bumps over a superhydrophobic surface. The hydrophilic bumps collect small water particles that accumulate and then roll over the super-hydrophobic regions down its limbs and head to sustain itself (Figure 2) ^[3]. The skin of the Texas Horned Lizard is also able to quickly absorb water with its pointed, textured hydrophilic surface (Figure 2) ^[4].

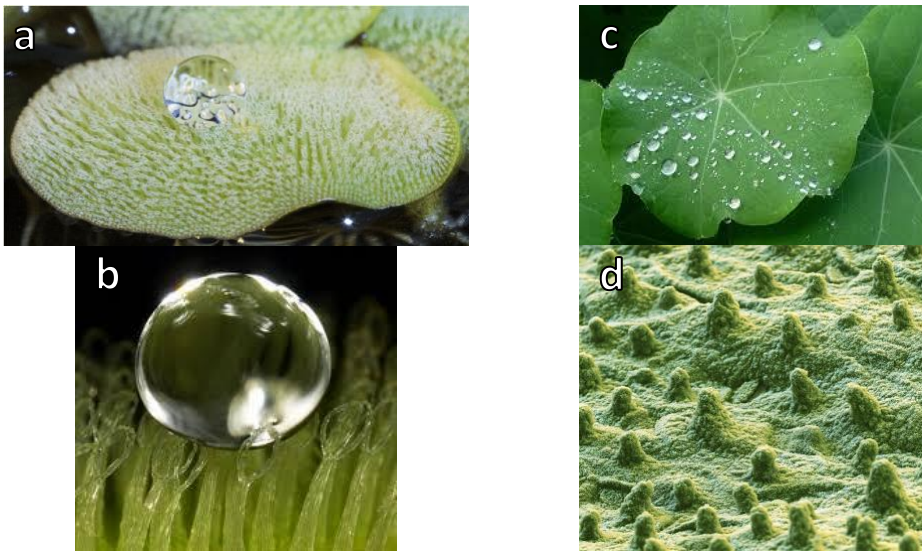


Figure 1. a-b). Water droplet on *Salvinia Molesta* plant ^[1]. c). Water droplets on *Nelumbo nucifera*, or the lotus plant leaf ^[2]. d). SEM image of *Nelumbo nucifera* surface ^[2].

Researchers who work in the area of biomimicry have duplicated the eggbeater-like shape of the *Salvinia Molesta* leaves on a micrometer scale using an immersed surface accumulation 3-D printer ^[1]. The structures were printed with a hydrophobic material with dimensions were that similar to those found on the plant. The 3-D printed model showed an effective mechanism for oil and water separation as shown in Figure 3. With the recent advances in the accessibility and capability of 3-D printing, this honors project was able to utilize the technology to achieve the small features observed in relevant research as well as natural surfaces.

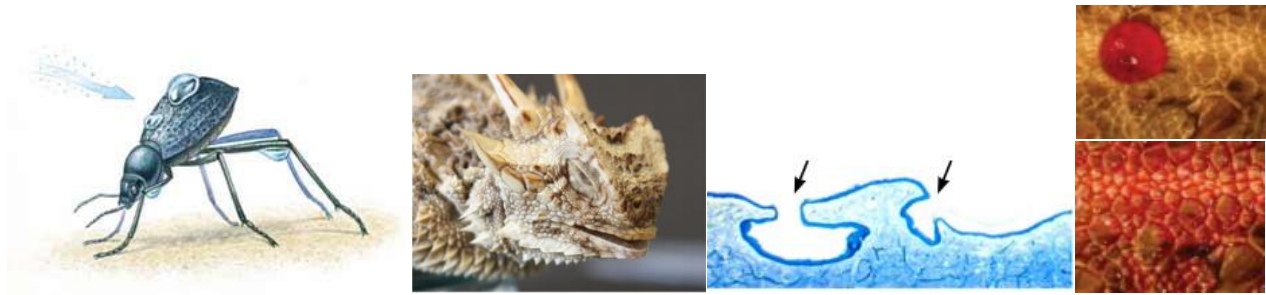


Figure 2. Left image: *Stenocara Gracilipes* desert beetle [3]. Right images: Texas horned lizard, or *Phrynosoma Cornutum*, and its skin structure. The water droplet shown easily wets the surface in seconds [4].



Figure 3. The time scale showing the separation of a water/oil mixture on the 3-D printed eggbeater features studied by Yang et al. Spacing between stalks was varied between 300-500 μm . The height of the stalks was 1000 μm and the diameter of the widest section was 300 μm [1].

The first goal of this honors project was to gain experience on how to fabricate 3D-printed featured surfaces with different geometries and modify them to achieve various surface wettability. The second goal was to examine the wetting transition on these featured surfaces and determine the surface characteristics that would completely prevent the porous features from being wet by a liquid. Insights gained from this project can potentially be applied to develop technology that can mitigate or even eliminate corrosion or can be used to trap water even in extreme conditions. Other useful applications would include self-cleaning surfaces, effective oil and water separation, water harvesting, anti-fogging and anti-fouling.

Background

The Wenzel and Cassie-Baxter equations (Equations 1 and 2 respectively) indicate that features can alter the contact angles (θ_{Wenzel} or $\theta_{\text{Cassie-Baxter}}$) from that of intrinsic contact angle (θ_s , see Figure 4a) of a liquid formed on a smooth surface of a particular material. In the Wenzel equation, r is the surface roughness factor and the liquid completely penetrates into grooves and wets the entire featured surface (Figure 4b) [5]. In the Cassie-Baxter case, f and $1-f$ are the area fractions occupied by the material and air, respectively. In this case, the liquid drop sits on top of the features, and the air trapped inside the grooves never gets replaced by the liquid (Figure 4c) [5].

$$\cos\theta_{\text{Wenzel}} = r\cos\theta_s \quad (1)$$

$$\cos\theta_{\text{Cassie-Baxter}} = f\cos\theta_s - (1 - f) \quad (2)$$

The criteria on whether or not a liquid drop can penetrate into the grooves to replace the trapped air can be predicted based on the following relationships. Equation 3 is the general criteria for liquid penetrating the grooves, or entering the Wenzel state, when $\theta_s < 90^\circ$. Equation

4 is the general criteria for air being trapped in the grooves, or the Cassie-Baxter state, when $\theta_s > 90^\circ$. θ_s is the contact angle of the flat surface. Not only can the wettability be predicted using these relationships, it also allows for tuning by adjusting the f_s and r parameters. F_s is ratio of the areas of the surface features to the total surface from an aerial view, while r is the ratio of the true surface area of the features to the aerial view total area of the surface. This means that r is also dependent on the height (H) of the features in addition to the diameter (D) and spacing (S) dependency shared by f_s . R is directly proportional to D and H and inversely proportional to S . F_s is directly proportional to D and inversely related to S . Thus, with a fixed contact angle less than 90° for a material, r should be decreased to obtain a more hydrophobic surface, so the left-hand side is less than the right-hand side (equation 3). With a fixed contact angle greater than 90° for a material, increasing r increases the likeliness for the surface to be hydrophobic (equation 4).

$$\cos\theta_s \geq \frac{1-f_s}{r-f_s} \quad \text{generally evaluated when } \theta_s < 90^\circ \quad (3)$$

$$\cos\theta_s \leq -\left(\frac{1-f_s}{r-f_s}\right) \quad \text{generally evaluated when } \theta_s > 90^\circ \quad (4)$$

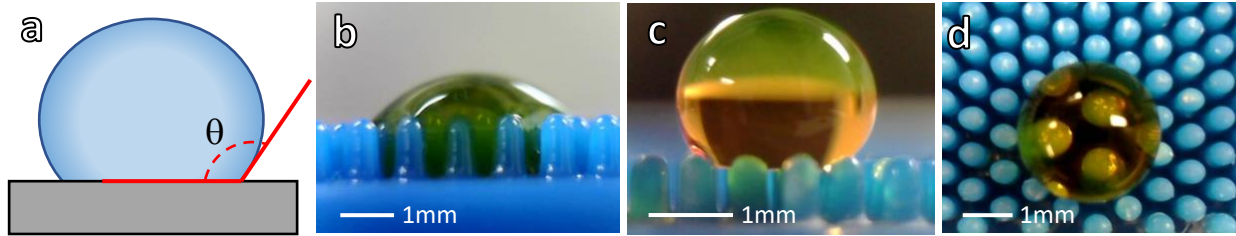


Figure 4. a). Contact angle of a droplet on a smooth surface. b). Droplet in the Wenzel state. c). Droplet in the Cassie-Baxter's state. d). Example aerial image used to calculate the radius of the droplet.

Generally, the contact angle of a liquid on a solid surface can be directly measured from the side view of the drop sitting on the surface, at its three-phase contact line. However, for some featured surfaces, the three-phase contact line is obstructed by the features. As a result, a top view of the drop (Figure 4d) might be used to relate the drop radius to the contact angle that the drop would form on the surface. Equation 5a relates the contact angle to the volume (V) and radius (R) of the droplet when the contact angle is less than 90° , while equation 5b is used when the contact angle is greater than 90° . In the application of this project, equation 5a-b were used to determine the contact angle, since V is known and R is easily measured. Also, to minimize the deformation due to the gravitational force, only drops with a volume of $\leq 10 \mu\text{L}$ were used (under which, the capillary number is less than the critical capillary number).

$$V = \frac{\pi}{3} R^3 (2 + \cos\theta)(1 - \cos\theta)^2 \quad \text{with } \theta < 90^\circ \quad (5a)$$

$$V = \frac{4\pi}{3} R^3 - \frac{\pi}{3} R^3 (2 - 3 \cos(180 - \theta) + \cos(180 - \theta)^3) \quad \text{with } \theta \geq 90^\circ \quad (5b)$$

Experimental Methods

Cylindrical pillars in a hexagonal array were 3D printed using the Stratasys Objet260 Connex3 polyjet printer with the curable photopolymer VeroCyan™ ink. The printer has a layer resolution of 16 μm and an accuracy of 200 μm . The pillar diameter (D) and pillar height (H) were varied from 300-500 μm and 1000-2000 μm respectively. The dimension ranges were decided after consideration of the analysis of the expected wetting of the surfaces (Table 1-2) as well as running print tests to find the limit for printer capability. The spacing (S) between the pillar bases was kept constant at 250 μm yet the spacing ratio (S/D) varied as a result. All of the models had a hexagonal array rather than a square array to increase the likeliness of the surface to be in the Cassie-Baxter state^[5]. Tests were run on four variations of the 3D surface; as printed, air plasma treated, OTS deposition, and inversed features in silicone polydimethylsiloxane (PDMS). The models were oxidized for 10 minutes at medium power in a Harrick Plasma Cleaner PDC-32G. When treated with OTS, the models were soaked in 40mL of HPLC grade hexane ($\geq 98.5\%$) with $\sim 2\text{mL}$ of 95% OTS for 30 minutes. The model's features were molded using the Sylgard® 184 silicone elastomer kit with a 10:1 weight ratio of the elastomer base to the curing agent. Water drops sitting on these surfaces were monitored via cameras, and images were captured at 0.5 s interval to determine whether and/or how fast the transition from the non-wetting state (i.e., Cassie-Baxter's state, when air fills the grooves/cavities) to the wetting state (i.e., Wenzel's state, when liquid penetrates the grooves) occurred. A standard droplet size of 10 μL was used, which was released using a VWR 2-20 μL pipette. Food coloring was added to water to visually distinguish the drop. The radius was calculated from the cross-sectional area of the droplet measured from the pictures taken. Then, along with the known volume of the droplet, the contact angle was calculated with equation 3. At least three runs were conducted for each model, with each treatment.

The initial experimental plan was to have all of the featured surfaces constructed with PDMS. The first obstacle encountered was that it was much more difficult for the 3D printer to print cavities than pillars at the desired level of resolution. This means to obtain the pillar features two successive moldings would be required. This was still attempted and there was little success due to the 3D polymer material poisoning two different curing agents for PDMS. Following this discovery, alternative materials to mold the 3D model were investigated such as 10 wt.% gelatin, polystyrene pellets, and polystyrene sheets. These also were not successful due to the gelatin having little toughness and the polystyrene being too brittle. Finally, the PDMS was able to cure using the OTS treated 3D model. A second mold to get the pillar features was not attempted at this time and the inverse features were studied.

Statistical analyses of runs were performed using a two-sample t-test that assumed unequal variances. A summary of the p-values from the t-tests comparing the models can be found in Appendix B.

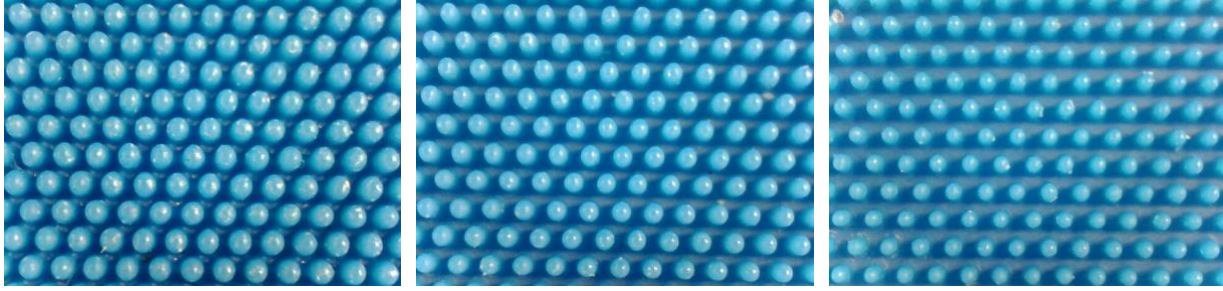


Figure 5. The aerial views of the 3-D model diameter variations studied. a. D500 H1000 S250 b. D400 H1000 S250 c. D300 H1000 S250. D, H, and S represent of pillar diameter, height, and spacing respectively. The number immediately following D, H or S is the dimension in μm .

Data and Results

Table 1 shows the parameters for the featured surfaces with cylindrical pillars along with the absolute value of the left-hand side quantity in equations 3 and 4. These quantities can be compared to the $\text{Cos}\theta_s$ values of the surfaces to predict the expected state of the model. The As Printed and Air Plasma Treated models are expected to transition to the Wenzel state, while the OTS treated surface is expected to remain in the Cassie-Baxter State.

Table 1. The calculations of r and f_s for the four models used in this project. D, R, S, and H represent the pillar diameter, radius, spacing, and height respectively. Three of the models had a height of $1000\mu\text{m}$ with varying diameters while one had a height of $2000\mu\text{m}$.

D (μm)	R (μm)	S+D (μm)	f_s	H (μm):	1000	H (μm):	2000
				r	$\left(\frac{1-f_s}{r-f_s}\right)$	r	$\left(\frac{1-f_s}{r-f_s}\right)$
300	150	550	0.270	4.60	0.169	-	-
400	200	650	0.343	4.43	0.160	-	-
500	250	750	0.403	4.22	0.156	7.45	0.08

Table 2. The measured apparent contact angles of water for the flat surfaces studied along with the cosine of the contact angle. The As Printed and Air Plasma Treated models, when evaluated with equation 3, are predicted to transition to the Wenzel state. The OTS treated and PDMS models, when evaluated with equation 4, are predicted to remain in the Cassie-Baxter State with the exception of the $300\mu\text{m}$ Diameter PDMS surface.

Surface	θ_s	$\text{Cos}\theta_s$
As Printed	75.3	0.253
Air Plasma Treated	33.7	0.832
OTS Treated	118.8	-0.482
PDMS	99.4	-0.163

The as printed model was hydrophilic due to the resin used being somewhat polar, which caused the droplets to easily wet the surface. As shown in Figure 6, when the diameter of the pillars decreased on the as printed model, the time to wet and the apparent contact angle

increased (Table 3). The height increase did not make a significant impact on the time to wet (blue vs. yellow bar Figure 6), even though the apparent contact angle increased (Table 3).

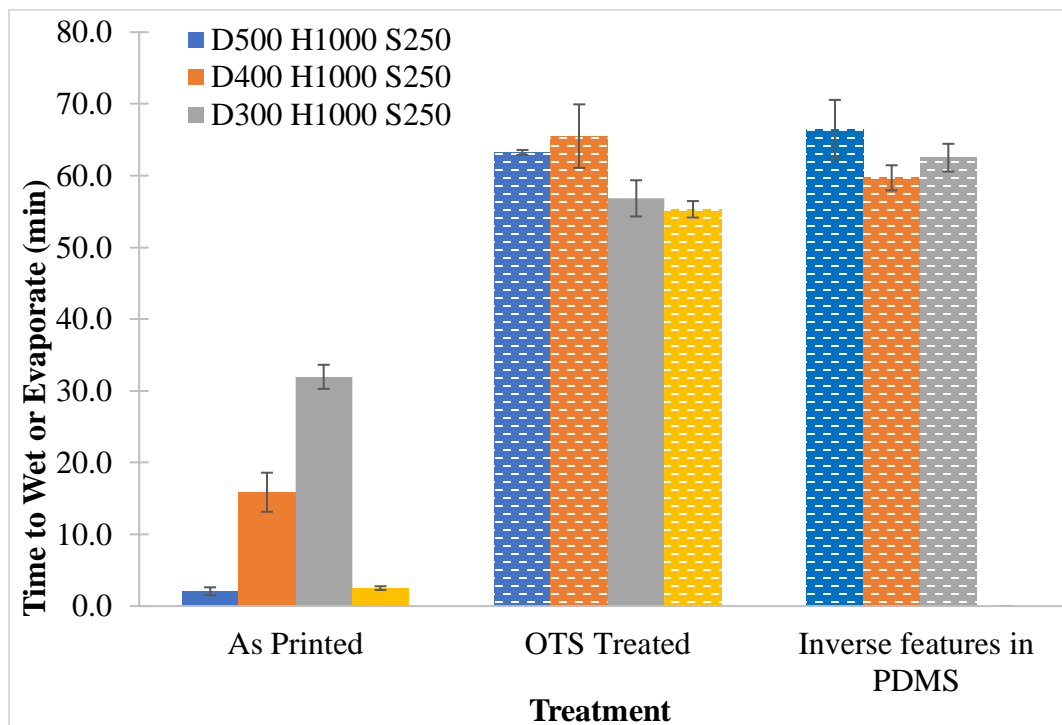


Figure 6. The time for water droplets to penetrate into the features for various models (for as printed models), or completely evaporate before observing water penetration into the features (dashed bars, for the OTS treated models and PDMS models with inversed features). The solid bar for the D300 H1000 S250 OTS treated indicated partial penetration of the water drop into the feature. The number immediately following D, H or S is the dimension in μm .

When the models were oxidized the surface became extremely hydrophilic as expected. The contact angle on the flat surface dropped from $76.1 \pm 5.8^\circ$ to a value of $33.7 \pm 8.6^\circ$, and the droplets wet the surface and penetrated into the features almost instantaneously. For the surface treatments that did not wet instantaneously, example time scales for the droplet behavior are depicted in Figure 7.

The OTS treatment prolonged water droplets from penetrating into the features. When changing the diameter from $500\mu\text{m}$ to $300\mu\text{m}$, some penetration of water droplets into the features was observed, which suggests the limit for a hydrophobic surface. The drop evaporated from the surface of the remaining models, and the height increase decreased the evaporation time (Figure 6) and significantly increased the contact angle (Table 3). Unlike the OTS treatment, all of the inversed features PDMS models resulted in the droplet evaporating and never wetting the cavities. The apparent water contact angle varied insignificantly for changes in diameter in models for the hydrophobic surface treatments (Table 3).

Estimated contact angles for all of the models were calculated using the Wenzel's and Cassie-Baxter's relations (equations 1-2), and are listed along with the measured value in Table 3. Details of the contact angle calculations can be found in Appendix A (Table A.2-3).

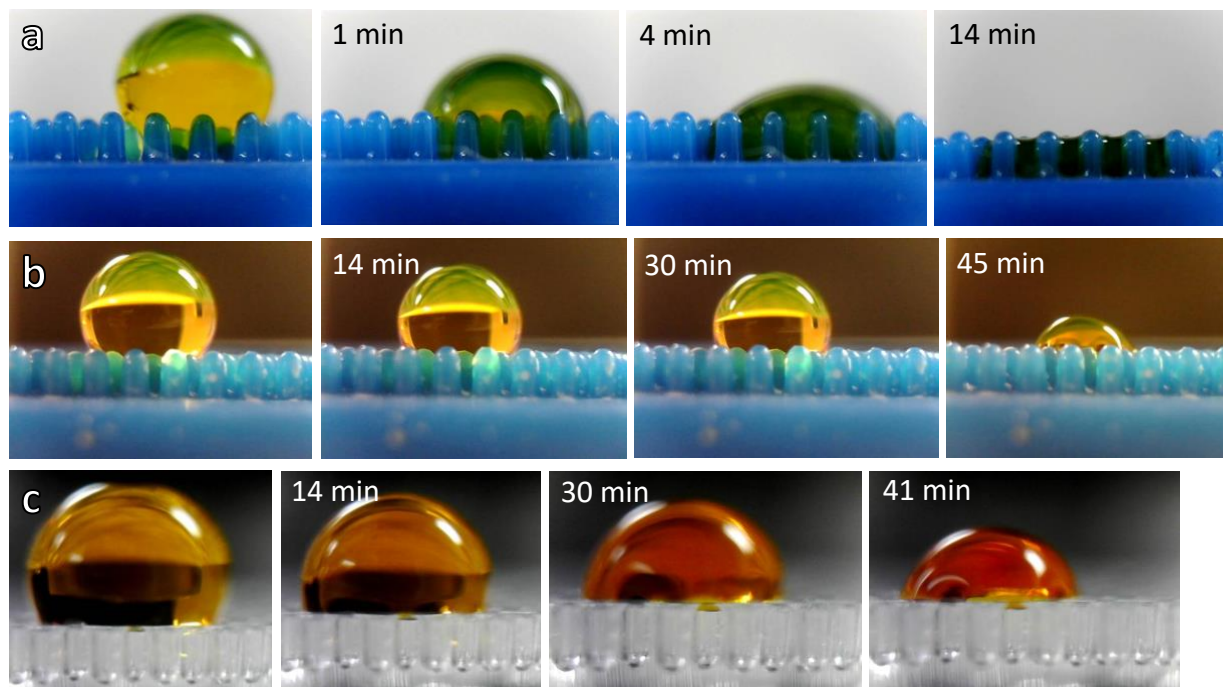


Figure 7. The time scale from when a 10 μL water droplet was initially placed on the surface of a a). D400 H1000 S250 as printed model b). D500 H1000 S250 OTS treated model c). D300 H1000 S250 inverse features in PDMS model.

Table 3. The Apparent water contact angles (in degrees) on the flat surfaces (of the polymer used for 3-D printing and PDMS) and models of various features summarized for the four treatments. The measured and estimated (equation 1-2) values are listed.

		Flat Surface	D500 H1000 S250	D400 H1000 S250	D300 H1000 S250	D500 H2000 S250
As Printed	Measured:	76.1 \pm 5.8	111.0 \pm 4.4	117.3 \pm 7.1	124.4 \pm 5.7	135.3 \pm 4.9
	Wenzel Estimation:	0				
	Cassie-Baxter Estimation:	120.0	125.0	131.7	120.0	
Air Plasma Treated	Measured:	33.7 \pm 8.6	~0, the droplets penetrated into the features instantaneously.			
	Wenzel Estimation:	0				
OTS Treated	Measured:	118.8 \pm 5.1	115.0 \pm 1.5	116.7 \pm 4.7	127.1 \pm 8.1	171.2 \pm 15.2
	Wenzel Estimation:	180				
	Cassie-Baxter Estimation:	142.3	145.3	149.3	142.3	
Inverse features in PDMS	Measured:	99.4 \pm 8.9	102.3 \pm 6.2	103.2 \pm 6.7	101.7 \pm 4.5	-
	Wenzel Estimation:	133.4	136.1	138.4	180	
	Cassie-Baxter Estimation:	131.5	135.4	140.7	131.5	

(Note: D, H, and S represent the pillar diameter, height, and spacing, respectively. The number immediately following each letter is its dimension in μm . There is no statistically significant difference between the water contact angles of the inversed features in PDMS. The apparent water contact angle was measured within 2s of placing the water drop on the surface).

Discussion and Analysis

The criteria for the Wenzel's state correlation (equation 3) were met for As Printed and Air Plasma Treated models. In all of the experimental runs, Wenzel's state correlation accurately predicted the transition to the droplet wetting the surface. The Wenzel's estimated contact angle (Table 3) of 0° for both models indicates a droplet completely spread over the surface, which was also supported by the experimental observation of the water droplet penetrating the grooves. Though the droplet eventually wet the surface of the As Printed models, the contact angles, measured right at the time when the droplet is placed on the surface, closely match the Cassie-Baxter's estimation.

The OTS treated and PDMS models, when evaluated with the Cassie-Baxter's state criteria (equation 4), were predicted to remain in the Cassie-Baxter's state with the exception of the 300 μm diameter PDMS surface. Experimentally, water droplets on the inverse features in PDMS models never penetrated the cavities while the D300 H1000 S250 OTS Treated model showed some droplet penetration into the features. Experimentally, the increase in height led to an increase in apparent water contact angle (from 115° to 171°) for the OTS treated model, indicating a superhydrophobic surface. Yet the estimated contact angle using the Cassie-Baxter's equation does not increase when the height increases, as the equation has no dependency on height. Only the Wenzel's equation varies with height due to the surface roughness. The observed contact angle trend could be due to slight penetration of the water droplet into the grooves as a result of the rounded tops of the cylindrical pillars. Therefore, the water droplet would not entirely be in Cassie-Baxter's state as indicated, but an intermediate state while the drop completely evaporated (still never wetting the surface), and surface roughness would have an effect.

A possible source for error in the measured contact angle could be a result of the volume of the water droplet being slightly less than the desired $10\mu\text{L}$. As a result, the radius measurement would inversely overestimate or underestimate the contact angle. The measured contact angle calculations also assume the shape of the droplet to be a perfect sphere, which would also contribute to error if that is not the case.

The geometry parameters, in the sub-millimeter to millimeter range we studied, for the inverse features in PDMS had little effect on the time for the droplet to penetrate (or more accurately not penetrate) into the grooves and had no effect on the apparent water contact angle. Thus, for the hydrophobic models, the surface wettability was more significant to water penetration into the porous features than the geometry, especially the inversed PDMS features (Table 3).

While it was our intention to generate much smaller feature sizes for this study, the 3D printer we used had size limitations. In order to obtain the desired small features, the spacing was not varied and the height could only be varied slightly. As a result, the variations of the r and f_s values were not as large as we had hoped for. In the future with a more capable 3D printer, it would be desirable to study surfaces with smaller pillar diameter, spacing, and varying heights, which would likely obtain more insightful results on the effects of features on liquid penetration. The 3D printer had additional printing limitations that resulted in the pillars having rounded tops

(see Figure 4a-b) instead of the desired flat tops. That downward angle contributed to the droplet more easily wetting the surface. This is ideal for a hydrophilic surface, but a flat or concave top would create a more liquid repelling surface ^[5].

Steps for further research would include investigating additional geometry dimensions and arrays, other liquids, and droplet volume. This research builds upon previous studies and technical reports concerning droplet behavior and surface features. Murakami et al. studied the transition of the Cassie-Baxter state to the Wenzel state with a hydrophobic cycloolefin polymer surface and liquids such as water and various ionic liquids. It was concluded that the transition state occurs when the energy barrier, primarily from the Laplace pressure, is overcome ^[6]. Lee et al. studied the wetting transition of water on cylindrical pillars in PDMS by only varying the spacing ratio. The diameter and height of the pillars was 105 microns and 150 microns, respectively, and the spacing was varied from 100-340 microns. As the spacing ratio increased the contact angle increased to a peak of $S/D \sim 2$ and then decreased. It was observed that the transition state occurred between a spacing ratio of $\sim 2-3$ ^[7].

The wetting transition of cavities in silicone oxide, a hydrophilic material, was studied and researchers found that a smaller intrinsic contact angle decreased the time to wet ^[8]. With the hydrophilic surface it was found that anionic, nonionic, and cationic surfactants had the highest to lowest cavity wetting rate ^[8]. There's significant research being done on this topic, and this project adds an additional perspective to the existing knowledge base.

Literature Cited

- [1] Yang, Y., Li, X., Zheng, X., Chen, Z., Zhou, Q., & Chen, Y. "3D-Printed Biomimetic Super-Hydrophobic Structure for Microdroplet Manipulation and Oil/Water Separation." *Advanced Materials*, vol. 30, 2018, pp. 1-11., doi:10.1002/adma.201704912.
- [2] Ensikat, Hans J et al. "Superhydrophobicity in perfection: the outstanding properties of the lotus leaf." *Beilstein journal of nanotechnology* vol. 2, 2011, pp. 152-61. doi:10.3762/bjnano.2.19
- [3] Nørgaard, T., and Dacke, M. "Fog-basking behavior and water collection efficiency in Namib Desert Darkling beetles." *Frontiers in zoology* vol. 7 23. 16, 2010, doi:10.1186/1742-9994-7-23
- [4] Comanns, P., Buchberger, G., Buchsbaum, A., Baumgartner, R., Kogler, A., Bauer, S., Baumgartner, W. "Directional, passive liquid transport: the Texas horned lizard as a model for a biomimetic 'liquid diode'". *J. R. Soc. Interface*, vol. 12, 2015. doi: 10.1098/rsif.2015.0415
- [5] Jung, K., Lee, D. "Fundamental Studies on Cassie equation and Cassie-Baxter to Wenzel Transition." *Graduate School of UNIST*. 2019.
- [6] Murakami, D., et al. "Wetting Transition from the Cassie–Baxter State to the Wenzel State on Textured Polymer Surfaces." *Langmuir*, vol. 30, no. 8, 2014, pp. 2061–2067. doi:10.1021/la4049067.

[7] Lee, J., Gwon, H., Lee, S., & Cho, M. “Wetting Transition Characteristics on Microstructured Hydrophobic Surfaces.” *Materials Transactions*, vol. 51 no. 9, 2010, pp 1709-1711., doi: 10.2320/matertrans.M2010118.

[8] Seo, D., et al. “Rates of Cavity Filling by Liquids.” *Proceedings of the National Academy of Sciences*, vol. 115, no. 32, 2018, pp. 8070–8075. doi:10.1073/pnas.1804437115.

Appendices

Appendix A: Additional Figures/Tables

Table A.1. The time (in minutes) to wet the models of various features are summarized. The grey boxes represent the models that the droplet did not penetrate the grooves in the surface and instead the droplet completely evaporated at the end of the monitoring period.

	D500 H1000 S250	D400 H1000 S250	D300 H1000 S250	D500 H2000 S250
As Printed	2.1±0.6	15.9±2.7	32.0±1.7	2.5±0.3
OTS Treated	63.2±0.3	65.5±4.4	56.8±2.5	55.3±1.1
Inverse features in PDMS	66.4±4.1	59.7±1.8	62.5±1.9	-

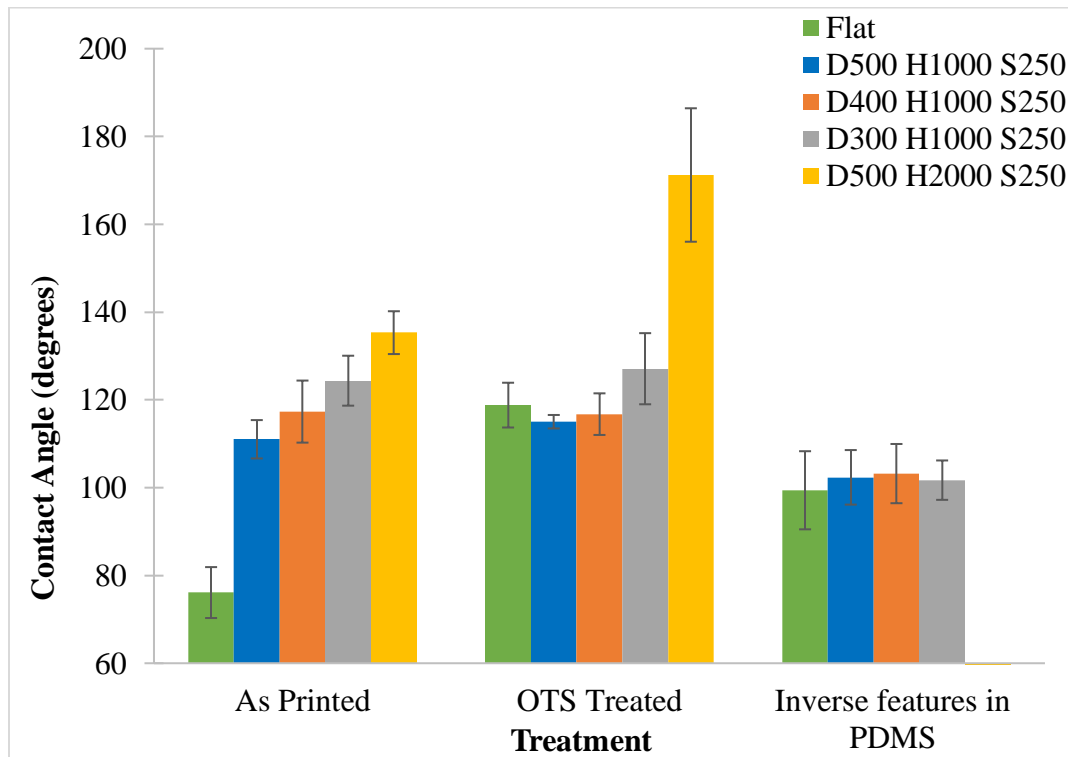


Figure A.1. The apparent water contact angles on the flat surfaces (of the polymer used for 3-D printing) and models of various features summarized for the four treatments.

Table A.2. The calculated values for the contact angle (in degrees) using the Wenzel's estimation (equation 1) of the features for the various treatments.

	As Printed		Air Plasma Treated		OTS Treated		Inverse Features in PDMS	
	cos θ	θ	cos θ	θ	cos θ	θ	cos θ	θ
D500 H1000 S250	1.015	Assume	3.513	Assume	-2.036	Assume	-0.687	133.4
D400 H1000 S250	1.066	0° since	3.688	0° since	-2.138	180° since	-0.721	136.1
D300 H1000 S250	1.105		3.823		-2.216		-0.748	138.4
D500 H2000 S250	1.790	cos $\theta > 1$	6.195	cos $\theta > 1$	-3.591	cos $\theta < -1$	-1.211	Assume 180°

Table A.3. The calculated values for the contact angle (in degrees) using the Cassie-Baxter's estimation (equation 2) of the features for the various treatments.

	As Printed		OTS Treated		Inverse Features in PDMS	
	cos θ	θ	cos θ	θ	cos θ	θ
D500 H1000 S250	-0.500	120.0	-0.791	142.3	-0.662	131.5
D400 H1000 S250	-0.574	125.0	-0.822	145.3	-0.712	135.4
D300 H1000 S250	-0.665	131.7	-0.860	149.3	-0.774	140.7
D500 H2000 S250	-0.500	120.0	-0.791	142.3	-0.662	131.5

Appendix B: Statistical Analysis and Results

The p-values from two-sample t-tests that assumed unequal variances. The green values indicate the models were significantly different from one another, while the red indicates that there was no difference observed in the values for those models.

Table B.1. The p-values for the comparison of the time to wet the As Printed models.

	D400 H1000 S250	D300 H1000 S250	D500 H2000 S250
D500 H1000 S250	0.7%	0.1%	11.7%
D400 H1000 S250	-	0.2%	0.7%
D300 H1000 S250	-	-	0.1%

Table B.2. The p-values for the comparison of the time to wet the OTS treated models.

	D400 H1000 S250	D300 H1000 S250	D500 H2000 S250
D500 H1000 S250	27.4%	2.4%	0.4%
D400 H1000 S250	-	1.1%	0.6%
D300 H1000 S250	-	-	20.5%

Table B.3. The p-values for the comparison of the time to wet the inverse features in PDMS.

	D400 H1000 S250	D300 H1000 S250
D500 H1000 S250	4.1%	28.4%
D400 H1000 S250	-	1.4%

Table B.4. The p-values for the comparison of the contact angles for the As Printed models.

	D400 H1000 S250	D300 H1000 S250	D500 H2000 S250
D500 H1000 S250	13.3%	1.4%	0.1%
D400 H1000 S250	-	12.5%	1.1%
D300 H1000 S250	-	-	3.2%

Table B.5. The p-values for the comparison of the contact angles for the OTS treated models.

	D400 H1000 S250	D300 H1000 S250	D500 H2000 S250
D500 H1000 S250	26.7%	6.3%	1.2%
D400 H1000 S250	-	7.1%	1.3%
D300 H1000 S250	-	-	1.1%

Table B.6. The p-values for the comparison of the contact angles for the inverse features in PDMS.

	D400 H1000 S250	D300 H1000 S250
D500 H1000 S250	21.0%	28.1%
D400 H1000 S250	-	38.5%